Transport and Communications Science Journal, Vol. 74, Issue 4 (05/2023), 544-556

Transport and Communications Science Journal

STABILITY OF MULTI-CRACKED FG PLATE ON ELASTIC FOUNDATIONS

Pham Minh Phuc, Le Vinh An*

University of Transport and Communications, No 3 Cau Giay Street, Hanoi, Vietnam

ARTICLE INFO

TYPE: Research Article
Received: 20/03/2023
Revised: 12/04/2023
Accepted: 14/05/2023
Published online: 15/05/2023
https://doi.org/10.47869/tcsj.74.4.13
* *Corresponding author*
Email: levinhan@utc.edu.vn

Abstract. Recently, the stability calculation of the functionally graded (FG) plate has attracted many scientists, especially when considering the FG plate with many cracks. In this work, the plate is made from a new generation composite material consisting of two components, ceramic and metal, with the law of continuous exponential material distribution. The plate is placed on a Winkler - Pasternak elastic foundation with two background parameters. Then, we used the third-order shear deformation plate theory to establish the dynamical equations. After applying Phase-Field theory to simulate the crack state, we applied the finite element method to solve the equations to find the critical force causing instability of the plate. Next, we investigated the influence of material index, number of cracks, crack length, crack shape as well as elastic foundation parameters on the plate stability. The results show that the crack length and elastic foundation parameter have the great influence on the stability of the FG plate. Especially, the elastic foundation with large shear coefficient, creating high stability for the plate. That is very meaningful in exploiting and using plate structure when the cracks appear.

Keywords: FG plate, multi-cracked plates, elastic foundation, Phase-Field theory, stability.

1. INTRODUCTION

Structural panels are widely used in practice as well as in engineering. In the field of transportation, the plates placed on an elastic foundation are commonly used in constructions such as pavement structures, bridge decks, etc. Therefore, in order to design and exploit this structure effectively, it is necessary to study the stability of the plate on different elastic bases. There are several authors who have researched on this issue. Hiroyuki [1] used the method of expanding the power series of displacement components derived from Hamilton's principle to

calculate the natural frequency and buckling stress of a dense isotropic plate placed on a Pasternak elastic foundation. Using the transformation of the Föppl–von Kármán equations, Takuya and Yoshinobu [2] studied the elastic stability of infinitely heterogeneous thin plates on a Winkler elastic foundation. Mehdi and Gholam [3] analyzed the buckling and free vibration of a plate on a Pasternak elastic foundation using the combination of the finite element method and the quadratic differential method.

The FG plate is a type of plate made from composite materials with many outstanding properties. When the FG plate is placed on an elastic foundation, its load-carrying capacity is much higher. The study of stability of this plate type placed on an elastic foundation has been mentioned by many studies. Huu-Tai and Seung-Eock [4] investigated the buckling of thick functionally graded plate resting on elastic foundation using the third-order shear deformation theory and the closed-form solution. Foroughi and Azhari [5] discussed the mechanical buckling and free vibration of rectangular FG plates on two-parameter elastic foundation due to the spline finite strip method approach and the third order shear deformation theory. Using hybrid higher-order shear and normal deformation theory and the variational principle, Gupta and Talha [6] determined the static and stability characteristics of geometrically imperfect FG plate resting on Pasternak elastic foundation. Singh and Harsha [7] employed the non-polynomial higher-order shear deformation theory with inverse hyperbolic shape function to analyse the free vibration and buckling characteristics of a sandwich FG plate resting on the Pasternak elastic foundation. Jędrysiak et al. [8] investigated the problem of the stability of FG thin plates using the tolerance model and the asymptotic model combined together with the Ritz method.

Although FG plate overcomes many limitations of multi-layer composite panels, defects such as cracks may still appear during production or use. In recent years, the calculation of the problem with cracks has attracted many scientists' attention. The studies have given a number of calculation methods for the structure with cracks such as: finite element method (FEM) [9], extended finite element method (XFEM) [10], A novel Ritz procedure [11], the XFEM combined with the discrete shear gap method (DSG) [12], ... Recently, the authors Phuc et al. [13-17] used the FEM method combined with phase field theory to study the stability and vibration of the plate with a crack.

According to the above review, no author has studied the stability of FG plates with many cracks placed on different elastic bases. The article will focus on calculating the stability parameter of the plate depending on the number of cracks, crack length, crack inclination angle, elastic foundation parameters as well as the ratio of material composition in the plate.

2. THE EQUATIONS

Here, the volume of the material components of the FG plate is changed according to the power law as in formula (1):

$$V_t = \left(\frac{z}{h} + \frac{1}{2}\right)^n ;\ V_b = 1 - V_t \tag{1}$$

where V_b and V_t are the volume fraction of bottom and top surfaces, respectively; n is the indicator according to the rule of power ($n \geq 0$) to determine the characteristic of changing materials along the thickness of the FG plate; z is the thickness coordinate variable

with $-h/2 \le z \le h/2$ and h is the thickness of the plates.

Rectangular plate made of FG materials with the properties can be rewritten as:

$$P = P_b + (P_t - P_b)V_t \tag{2}$$

where P is the property of the FG material at any position z; P_b and P_t are the material properties of bottom and top sides, respectively. In this study, P is Young's modulus and Poisson's ratio.

This research introduces a finite element formula for the plate using Shi's the third-order shear deformation theory [18] based on the strict kinematic assumption of displacement. It can be seen that the kinematics of the displacement which is derived from the elastic formula is closer to the finite element method than from the displacement hypothesis. The displacements (U_x, U_y, U_z) at any point $\mathrm{M}(x, y, z)$ in the plate can be represented as five unknown variables as expression (3):

$$\begin{aligned}
U_x(x,y,z) &= U_{0x}(x,y) + \frac{5}{4}\left(z - \frac{4}{3h^2}z^3\right)\alpha_x(x,y) + \left(\frac{1}{4}z - \frac{5}{3h^2}z^3\right)\frac{\partial U_{0z}(x,y)}{\partial x} \\
U_y(x,y,z) &= U_{0y}(x,y) + \frac{5}{4}\left(z - \frac{4}{3h^2}z^3\right)\alpha_y(x,y) + \left(\frac{1}{4}z - \frac{5}{3h^2}z^3\right)\frac{\partial U_{0z}(x,y)}{\partial y} \\
U_z(x,y,z) &= U_{0z}(x,y)
\end{aligned} \tag{3}$$

The deformation components:

$$\begin{Bmatrix} \boldsymbol{\varepsilon}_x \\ \boldsymbol{\varepsilon}_y \\ \boldsymbol{\varepsilon}_{xy} \\ \boldsymbol{\gamma}_{yz} \\ \boldsymbol{\gamma}_{xz} \end{Bmatrix} = \begin{Bmatrix} U_{0x,x} + z\frac{1}{4}(5\alpha_{x,x} + U_{z,xx}) + z^3\left(\frac{-5}{3h^2}\right)\left[\alpha_{x,x} + U_{z,xx} + \left(\frac{-2}{h}\right)h_{,x}\left(\alpha_x + U_{z,x}\right)\right] \\ U_{0y,y} + z\frac{1}{4}(5\alpha_{y,y} + U_{z,yy}) + z^3\left(\frac{-5}{3h^2}\right)(\alpha_{y,y} + U_{z,yy}) \\ U_{0x,y} + U_{0y,x} + z\frac{1}{4}(5\alpha_{x,y} + 2U_{z,xy} + 5\alpha_{y,x}) + \\ \qquad + z^3\left(\frac{-5}{3h^2}\right)\left[\alpha_{x,y} + 2U_{z,xy} + \alpha_{y,x} + \left(\frac{-2}{h}\right)h_{,x}\left(\alpha_y + U_{z,y}\right)\right] \\ \frac{5}{4}(\alpha_y + U_{z,y}) + z^2\left(\frac{-5}{h^2}\right)(\alpha_y + U_{z,y}) \\ \frac{5}{4}(\alpha_x + U_{z,x}) + z^2\left(\frac{-5}{h^2}\right)(\alpha_x + U_{z,x}) \end{Bmatrix} \tag{4}$$

Where U_x, U_y, U_z are the displacements at the middle plane of the plate in the x, y, z axes, respectively; α_x, α_y are the normal rotation angles of the mid-plate along the x, y axes. The commas describe the derivatives corresponding to the variables x, y.

The relationship of strain and stress components is shown through the following expressions:

$$\begin{cases} \boldsymbol{\sigma} = \bar{\boldsymbol{D}}_m(\boldsymbol{\varepsilon}_0 + z\boldsymbol{\varepsilon}_1 + z^3\boldsymbol{\varepsilon}_3) \\ \boldsymbol{\tau} = \bar{\boldsymbol{D}}_s(\boldsymbol{\gamma}_0 + z^2\boldsymbol{\gamma}_2) \end{cases} \tag{5}$$

with $\boldsymbol{\sigma} = \begin{bmatrix} \sigma_x & \sigma_y & \sigma_{xy} \end{bmatrix}^T$; $\boldsymbol{\tau} = \begin{bmatrix} \tau_{yz} & \tau_{xz} \end{bmatrix}^T$

$$\bar{\boldsymbol{D}}_m = \frac{E}{1-\upsilon^2}\begin{bmatrix} 1 & \upsilon & 0 \\ \upsilon & 1 & 0 \\ 0 & 0 & \frac{1}{2}(1-\upsilon) \end{bmatrix};\ \bar{\boldsymbol{D}}_s = \frac{E}{2(1+\upsilon)}\begin{bmatrix} 1 & 0 \\ 0 & 1 \end{bmatrix} \tag{6}$$

where E is Young's modulus; υ is the Poisson's ratio. And note that the symbol $\boldsymbol{\varepsilon}_0; \boldsymbol{\varepsilon}_1; \boldsymbol{\varepsilon}_3; \boldsymbol{\gamma}_0; \boldsymbol{\gamma}_2$ in equation (5) is the strain components in equation (4) of the displacements in the plate [18].

The components of normal force, bending moment, higher-order moment and shear force according to the HSDT of Shi [18] are introduced according to the equations:

$$\begin{Bmatrix} \bar{\boldsymbol{N}} \\ \bar{\boldsymbol{M}} \\ \bar{\boldsymbol{P}} \\ \bar{\boldsymbol{Q}} \\ \bar{\boldsymbol{R}} \end{Bmatrix} = \begin{bmatrix} \hat{\boldsymbol{A}} & \hat{\boldsymbol{B}} & \hat{\boldsymbol{E}} & 0 & 0 \\ \hat{\boldsymbol{B}} & \hat{\boldsymbol{D}} & \hat{\boldsymbol{F}} & 0 & 0 \\ \hat{\boldsymbol{E}} & \hat{\boldsymbol{F}} & \hat{\boldsymbol{H}} & 0 & 0 \\ 0 & 0 & 0 & \boldsymbol{A} & \boldsymbol{B} \\ 0 & 0 & 0 & \boldsymbol{B} & \boldsymbol{D} \end{bmatrix} \begin{Bmatrix} \boldsymbol{\varepsilon}_0 \\ \boldsymbol{\varepsilon}_1 \\ \boldsymbol{\varepsilon}_3 \\ \boldsymbol{\gamma}_0 \\ \boldsymbol{\gamma}_2 \end{Bmatrix} \tag{7}$$

$$\text{where } (\hat{\boldsymbol{H}}, \hat{\boldsymbol{F}}, \hat{\boldsymbol{E}}, \hat{\boldsymbol{D}}, \hat{\boldsymbol{B}}, \hat{\boldsymbol{A}}) = \int_{-h/2}^{h/2} (z^6, z^4, z^3, z^2, z, 1)\bar{\boldsymbol{D}}_m dz;\ (\boldsymbol{D}, \boldsymbol{B}, \boldsymbol{A}) = \int_{-h/2}^{h/2} (z^4, z^2, 1)\bar{\boldsymbol{D}}_s dz \tag{8}$$

On the basis of elastic theory, the strain energy of the plate (W) can be written as:

$$\mathrm{W}(\boldsymbol{q}) = \frac{1}{2}\int_\Omega \begin{pmatrix} \boldsymbol{\varepsilon}_0^{\mathrm{T}}\hat{\boldsymbol{A}}\boldsymbol{\varepsilon}_0^{\mathrm{T}} + \boldsymbol{\varepsilon}_0^{\mathrm{T}}\hat{\boldsymbol{B}}\boldsymbol{\varepsilon}_1 + \boldsymbol{\varepsilon}_0^{\mathrm{T}}\hat{\boldsymbol{E}}\boldsymbol{\varepsilon}_3 + \\ + \boldsymbol{\varepsilon}_1^{\mathrm{T}}\hat{\boldsymbol{B}}\boldsymbol{\varepsilon}_0 + \boldsymbol{\varepsilon}_1^{\mathrm{T}}\hat{\boldsymbol{D}}\boldsymbol{\varepsilon}_1 + \boldsymbol{\varepsilon}_1^{\mathrm{T}}\hat{\boldsymbol{F}}\boldsymbol{\varepsilon}_3 + \\ + \boldsymbol{\varepsilon}_3^{\mathrm{T}}\hat{\boldsymbol{E}}\boldsymbol{\varepsilon}_0 + \boldsymbol{\varepsilon}_3^{\mathrm{T}}\hat{\boldsymbol{F}}\boldsymbol{\varepsilon}_1 + \boldsymbol{\varepsilon}_3^{\mathrm{T}}\hat{\boldsymbol{H}}\boldsymbol{\varepsilon}_3 + \\ + \boldsymbol{\gamma}_0^{\mathrm{T}}\boldsymbol{A}\boldsymbol{\gamma}_0 + \boldsymbol{\gamma}_0^{\mathrm{T}}\boldsymbol{B}\boldsymbol{\gamma}_2 + \boldsymbol{\gamma}_2^{\mathrm{T}}\boldsymbol{B}\boldsymbol{\gamma}_0 + \boldsymbol{\gamma}_2^{\mathrm{T}}\boldsymbol{D}\boldsymbol{\gamma}_2 \end{pmatrix} \mathrm{d}\Omega \tag{9}$$

where $\mathrm{W}(\boldsymbol{q})$ is the potential energy of the plate in the absence of cracks; $\boldsymbol{q}$ is displacement vector.

The energy of the Pasternak elastic foundation acting on the plate:

$$\mathrm{W}^e(\boldsymbol{q}, s) = \frac{1}{2}\int_\Omega s^2 \left\{ k_w U_z^2 + k_s \left[\left(\frac{\partial U_z}{\partial x} \right)^2 + \left(\frac{\partial U_z}{\partial y} \right)^2 \right] \right\} d\Omega \tag{10}$$

with k_w, k_s are the coefficients of the elastic foundation Pasternak. In the case of the plate supported on a Winkler foundation, k_s is zero.

To simulate the state of a material, phase field theory introduces a scalar variable s. When the material is in the crack region, the variable s is between 0 and 1. For the material in the fully cracked state, s=0. In contrast, for a material in its normal state, s=1. In the strain energy expression, the variable s is added to show that when the plate is cracked, the energy is reduced.

The total strain energy for the plate can be determined by equation (11):

$$
\begin{aligned}
\mathrm{W}^t(\boldsymbol{q},s) &= \mathrm{W}(\boldsymbol{q},s)+\mathrm{W}^e(\boldsymbol{q},s) \\
&= \left\{ \begin{array}{l}
\dfrac{1}{2}\displaystyle\int_\Omega s^2 \left(\begin{array}{l}
\boldsymbol{\varepsilon}_0^T \hat{\boldsymbol{A}} \boldsymbol{\varepsilon}_0^T + \boldsymbol{\varepsilon}_0^T \hat{\boldsymbol{B}} \boldsymbol{\varepsilon}_1 + \boldsymbol{\varepsilon}_0^T \hat{\boldsymbol{E}} \boldsymbol{\varepsilon}_3 + \\
+\boldsymbol{\varepsilon}_1^T \hat{\boldsymbol{B}} \boldsymbol{\varepsilon}_0 + \boldsymbol{\varepsilon}_1^T \hat{\boldsymbol{D}} \boldsymbol{\varepsilon}_1 + \boldsymbol{\varepsilon}_1^T \hat{\boldsymbol{F}} \boldsymbol{\varepsilon}_3 + \\
+\boldsymbol{\varepsilon}_3^T \hat{\boldsymbol{E}} \boldsymbol{\varepsilon}_0 + \boldsymbol{\varepsilon}_3^T \hat{\boldsymbol{F}} \boldsymbol{\varepsilon}_1 + \boldsymbol{\varepsilon}_3^T \hat{\boldsymbol{H}} \boldsymbol{\varepsilon}_3 + \\
+\boldsymbol{\gamma}_0^T \boldsymbol{A} \boldsymbol{\gamma}_0 + \boldsymbol{\gamma}_0^T \boldsymbol{B} \boldsymbol{\gamma}_2 + \boldsymbol{\gamma}_2^T \boldsymbol{B} \boldsymbol{\gamma}_0 + \boldsymbol{\gamma}_2^T \boldsymbol{D} \boldsymbol{\gamma}_2
\end{array} \right) d\Omega + \\
+\dfrac{1}{2}\displaystyle\int_\Omega s^2 \left\{ k_w U_z^2 + k_s \left[\left(\dfrac{\partial U_z}{\partial x} \right)^2 + \left(\dfrac{\partial U_z}{\partial y} \right)^2 \right] \right\} d\Omega + \\
+\dfrac{1}{2}\displaystyle\int_\Omega s^2 \left[U_{z,x} \quad U_{z,y} \right] \tilde{\sigma}^0 \left[U_{z,x} \quad U_{z,y} \right]^T h d\Omega + \\
+\dfrac{1}{2}\displaystyle\int_\Omega s^2 \left[\alpha_{x,x} \quad \alpha_{x,y} \right] \tilde{\sigma}^0 \left[\alpha_{x,x} \quad \alpha_{x,y} \right]^T \dfrac{h^3}{12} d\Omega + \\
+\dfrac{1}{2}\displaystyle\int_\Omega s^2 \left[\alpha_{y,x} \quad \alpha_{y,y} \right] \tilde{\sigma}^0 \left[\alpha_{y,x} \quad \alpha_{y,y} \right]^T \dfrac{h^3}{12} d\Omega + \\
+\displaystyle\int_\Omega G_C h \left[\dfrac{(1-s)^2}{4 l_c} + l_c |\nabla s|^2 \right] d\Omega
\end{array} \right. \\
&= \left\{ \int_\Omega s^2 \Lambda(\boldsymbol{q}) d\Omega + \int_\Omega G_C h \left[\dfrac{(1-s)^2}{4 l_c} + l_c |\nabla s|^2 \right] d\Omega \right\}
\end{aligned}
\tag{11}
$$

where G_C is surface energy in Griffith's theory and l_c is a positive constant used to represent the crack width.

$$
\bar{\sigma}^0 = \begin{bmatrix} \bar{\sigma}_x^0 & \bar{\tau}_{xy}^0 \\ \bar{\tau}_{xy}^0 & \bar{\sigma}_y^0 \end{bmatrix} \tag{12}
$$

with $\bar{\sigma}_x^0$, $\bar{\sigma}_y^0$ are the normal stresses of the plate for the x, y axes, respectively; $\bar{\tau}_{xy}^0$ is the shear stress of the plate in the x-y plane, at the time of external forces acting on the plate edges.

The first-order variation of function $\mathrm{W}^t(\boldsymbol{q},s)$ with respect to variables $\boldsymbol{q},s$ is defined by formula (13) as follows:

$$\begin{cases}\delta \mathrm{W}^t(\boldsymbol{q},s,\delta\boldsymbol{q})=0\\ \delta \mathrm{W}^t(\boldsymbol{q},s,\delta s)=0\end{cases} \tag{13}$$

From equation (13), the equations for calculating the instability of the cracked plate are shown as follows:

$$\left(\sum \mathbf{K}^e+\eta_{cr}\sum \mathbf{K}_G^e\right)\boldsymbol{q}=0 \tag{14}$$

$$\int_\Omega 2s\Lambda(\boldsymbol{q})\delta s d\Omega+\int_\Omega 2G_C h\left[-\frac{(1-s)}{4l_c}+l_c\nabla s\nabla(\delta s)\right]d\Omega=0 \tag{15}$$

Substituting the value of s calculated from equation (15) into equation (14), we can find the critical buckling load η_{cr}. In Equation (15), the shape of the crack is described by the function $\Lambda(\boldsymbol{q})$ according to Borden et al. [19] as follows:

$$\Lambda(\boldsymbol{q})=10^3\frac{G_C}{4l_c}.\mathrm{T}_0(x,y) \text{ where} \tag{16}$$

$$T_0(x,y)=\begin{cases}\left(1-\dfrac{d(x,y)}{l_c}\right) & if\ \dfrac{-c.\sin\psi}{2}\le x-\dfrac{L}{2}\le\dfrac{c.\sin\psi}{2}\ \ and\ \ \dfrac{-l_c}{2}\le y-\dfrac{H}{2}+\left(x-\dfrac{L}{2}\right)\cot\psi\le\dfrac{l_c}{2}\\ 0 & else\end{cases}$$

where ψ and c are the crack inclination angle and length (Fig. 1), respectively; l_c is the width of the crack; $d(x,y)$ is the minimum distance from any point (x,y) to the crack boundary; L and H are the dimensions of the two sides of the plate.

3. THE RESULTS AND DISCUSSION

3.1. Comparison results

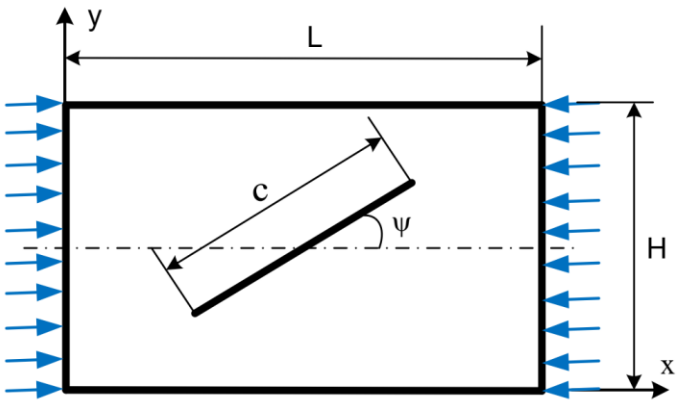

Figure 1. The geometry of cracked FG plate under uniaxial compression load in x direction.

In this section, the rectangular cracked FG plates studied by Liu et al [12] is considered here for comparison. The plate have *L*= *H* = 0.4*m*, *L/h*=100 and the material properties: Young's modulus, the Poisson's ratio of Aluminium (*Al*) and Zirconium dioxide (ZrO_2) are $E_m = 70GPa, \upsilon_m = 0.3$ and $E_c = 151GPa, \upsilon_c = 0.3$, respectively. The plate has the simply support boundary condition on four edges (*SSSS*). The formula for determining the buckling parameter of the FG plate according to Liu et al [12]:

$$\kappa_c = \frac{\eta_{cr} H^2}{\pi^2 D_c} \quad \text{where} \quad D_c = \frac{E_c h^3}{12(1-\upsilon_c^2)}. \tag{17}$$

Table 1. Stability coefficient of square FG plate with one crack and boundary condition *SSSS.*

	n	*c/L*			
		0.2	0.4	0.6	0.8
Liu et al. [12]	0	3.8263	3.4038	2.9995	2.7425
This study		3.75591	3.33145	2.96234	2.74705
Diff.		-1.84%	-2.13%	-1.24%	0.17%
Liu et al. [12]	0.2	3.3865	3.0128	2.6548	2.4272
This study		3.33751	2.96043	2.63244	2.4411
Diff.		-1.45%	-1.74%	-0.84%	0.57%
Liu et al. [12]	0.5	2.9937	2.6635	2.347	2.1456
This study		2.95251	2.61899	2.32885	2.15955
Diff.		-1.38%	-1.67%	-0.77%	0.65%
Liu et al. [12]	1	2.6757	2.3806	2.0977	1.9177
This study		2.63633	2.33852	2.07945	1.92828
Diff.		-1.47%	-1.77%	-0.87%	0.55%
Liu et al. [12]	2	2.4521	2.1813	1.9222	1.7575
This study		2.41472	2.14184	1.90453	1.76612
Diff.		-1.52%	-1.81%	-0.92%	0.49%
Liu et al. [12]	5	2.2742	2.0227	1.7825	1.6302
This study		2.24477	1.9909	1.77028	1.64168
Diff.		-1.29%	-1.57%	-0.69%	0.70%
Liu et al. [12]	10	2.1372	1.9007	1.6751	1.532
This study		2.11618	1.87682	1.66883	1.54761
Diff.		-0.98%	-1.26%	-0.37%	1.02%

The numerical results here are compared with the study of Liu et al. [12]. It can be seen that, with the small difference as shown in Table 1, it proves the reliability of the calculation method and program. On that basis, we develop a calculation program based on these codes to study the stability of cracked FG plates lying on the elastic foundations in Section 3.2 below.

3.2. Stability of FG plate with many cracks on elastic foundation

In this section, the buckling coefficients of cracked FG plates with length (*L*), width $H = 0.4m$ and thickness $h = 4mm$. The FG plate made of Aluminium (*Al*) and Zirconium dioxide (ZrO_2) with Young's modulus and Poisson's ratio are the same as in section 3.1. The

plate is placed on the two-parameter elastic foundation (Pasternak foundation) and the crack is assumed to be a straight line as shown in Figure 2. The stability factor is analyzed based on the change of number of cracks, the length and location of the crack, the crack length (*c*) varies from 0 to 80% of the plate length. The boundary condition of the plate is full simple support (*SSSS*) when subjected to uniaxial compressive loads on opposite sides in the x-axis. The buckling coefficient is calculated according to the following formula (17).

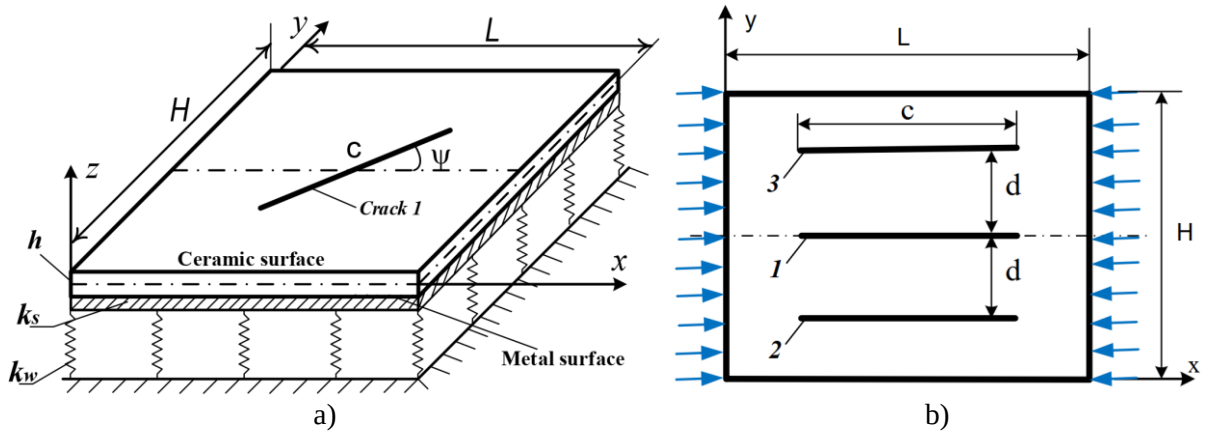

Figure 2. The cracked FG plate resting on elastic foundation: a) with 1 crack; b) with many cracks.

Here, the corresponding unitless elastic foundation coefficients according to the formula (18):

$$\tilde{k}_w = \frac{k_w L^4}{D_c};\ \tilde{k}_s = \frac{k_s L^2}{D_c} \text{ with } D_c = \frac{E_c h^3}{12(1-\upsilon^2)} \tag{18}$$

In case the FG plate has a crack (Fig. 2a), the crack is located in the center of the plate with the inclined angles investigated in the different cases 0 degrees, 30 degrees and 60 degrees.

Table 2. Effect of crack length and angle, power-law index on the stability coefficient of FG plate (L/H = 1.25; H/h = 100; $\tilde{k}_w = 50; \tilde{k}_s = 15$; *SSSS*).

		Power-law index (*n*)						
c/H	ψ^0	0	0.2	0.5	1	2	5	10
0	-	6.41372	5.85919	5.34897	4.93011	4.63669	4.41184	4.24157
0.2		6.41331	5.85888	5.34878	4.92997	4.63663	4.41182	4.24154
0.4	0	6.36892	5.81979	5.31456	4.89973	4.60915	4.38644	4.21776
0.6		5.90742	5.57271	5.17922	4.77958	4.49958	4.2849	4.12238
0.2		6.41371	5.85917	5.34896	4.93007	4.63666	4.4118	4.24147
0.4	30	6.2136	5.82623	5.32588	4.90936	4.61755	4.39384	4.22444
0.6		5.66392	5.33867	5.03742	4.81136	4.52797	4.3106	4.14609
0.2		6.41318	5.85858	5.34831	4.92936	4.6359	4.41097	4.24061
0.4	60	5.91875	5.51515	5.13508	4.81304	4.57915	4.40969	4.23856
0.6		5.02269	4.69054	4.37829	4.11497	3.92511	3.77561	3.66066

The numerical results presented in Table 2 show that as the power-law index (n) increases, the metal content in the sheet increases, leading to a decrease in the stiffness of the plate and a corresponding decrease in the critical buckling load. As the crack length (ψ) increases, the stiffness of the plate decreases, which obviously causes a gradual decrease in the critical instability load. In addition, the increase in crack inclination significantly affects the buckling load, which decreases slightly when the angle of inclination is from 0 to 30 degrees, but decreases more strongly when the angle of inclination increases from 30 to 60 degrees.

In the case of FG plate with many cracks, it is assumed that the cracks are parallel to the x axis (Fig. 2b). The plate has two cracks described as crack 2 and crack 3, they are separated from the center axis by a distance *d*.

Table 3. Stability coefficient of FG plate with two cracks with different elastic foundation (*L/H* = 1.5; *H/h* = 100; *n* = 2; *SSSS*).

		$(\tilde{k}_w, \tilde{k}_s)$						
c/H	*d/H*	(50,0)	(100,0)	(0,10)	(0,20)	(50,10)	(50,20)	(100,50)
0	-	2.84527	2.90229	3.49171	4.19517	3.54873	4.25219	6.41958
0.2		2.87244	2.93009	3.52123	4.22766	3.57888	4.28531	6.46208
0.4	0.1	2.43892	2.64351	3.49659	4.20526	3.55446	4.26312	6.44651
0.6		2.03484	2.24051	3.17465	4.06849	3.41838	4.12555	6.29634
0.2		2.86005	2.91753	3.5081	4.21362	3.56558	4.2711	6.44505
0.4	0.2	2.51989	2.7254	3.4825	4.18839	3.54012	4.246	6.42007
0.6		2.06613	2.26907	3.07429	4.05082	3.24617	4.10769	5.93362
0.2		2.84486	2.90213	3.49199	4.19638	3.54925	4.25364	6.424
0.4	0.3	2.7136	2.87953	3.46764	4.1701	3.52497	4.22741	6.39005
0.6		2.22383	2.42036	3.08916	3.88492	3.24859	3.99563	5.70284

In the subsequent analysis as described in Table 3, the larger the crack length, the lower the critical buckling load. As the distance between the two cracks increases, i.e. the crack position is further away from the center, the ultimate buckling load will increase. It should be noted that the crack is the energy release zone inside the plate, the instability phenomenon when the plate has a crack in the center is much more likely to occur than in the case of a plate with a crack far away from the center. In particular, the elastic foundation has a great influence on the stability of the plate. When the elastic foundation coefficient increases, the stiffness of the plate increases, causing the critical buckling load to increase. We also see that the shear resistance coefficient (k_s) has a greater influence on the unstable load than the Winkler foundation coefficient (k_w).

In the subsequent analysis, when gradually increasing the crack length or gradually decreasing the elastic foundation coefficients, it is easy to see that the critical buckling load decreases as shown in Table 4. However, in the experiment when changing the distance between the cracks (d) as shown in Figure 2b, the larger the distance between the two outer cracks (cracks: 2 and 3), the greater the critical load, this is only true for the panels placed on the Winkler foundation and *c/H*=0.4 or *c/H*=0.6. It is worth noting that when the plate is placed on the Pasternak foundation, the shear resistance parameter (k_s) significantly reduces the influence of the crack location, which is also shown in Table 3.

Table 4. Stability coefficient of square FG plate with three cracks with H/h = 100; n = 1; *SSSS*.

		$(\tilde{k}_w, \tilde{k}_s)$						
c/H	*d/H*	(50,0)	(100,0)	(0,10)	(0,20)	(50,10)	(50,20)	(100,50)
0.3		2.74913	3.23683	4.28778	6.30006	4.77455	6.78358	11.0488
0.5	0.1	2.41761	2.90124	3.92953	5.8489	4.40862	6.31772	10.7208
0.7		2.22477	2.71391	3.64684	5.38866	4.12787	5.85361	10.1974
0.3		2.7405	3.23274	4.23858	6.19999	4.72888	7.16682	11.006
0.5	0.2	2.35269	2.84054	3.71903	5.44609	4.19885	6.37079	10.5956
0.7		2.09293	2.58547	3.25157	4.71343	3.73427	5.64939	9.36233
0.3		2.80775	3.3045	4.26696	6.17884	4.76141	6.66719	10.9639
0.5	0.3	2.36701	2.85867	3.62202	5.22485	4.10522	5.69396	10.2343
0.7		2.03986	2.5359	3.0481	4.38593	3.53642	4.86558	8.88809

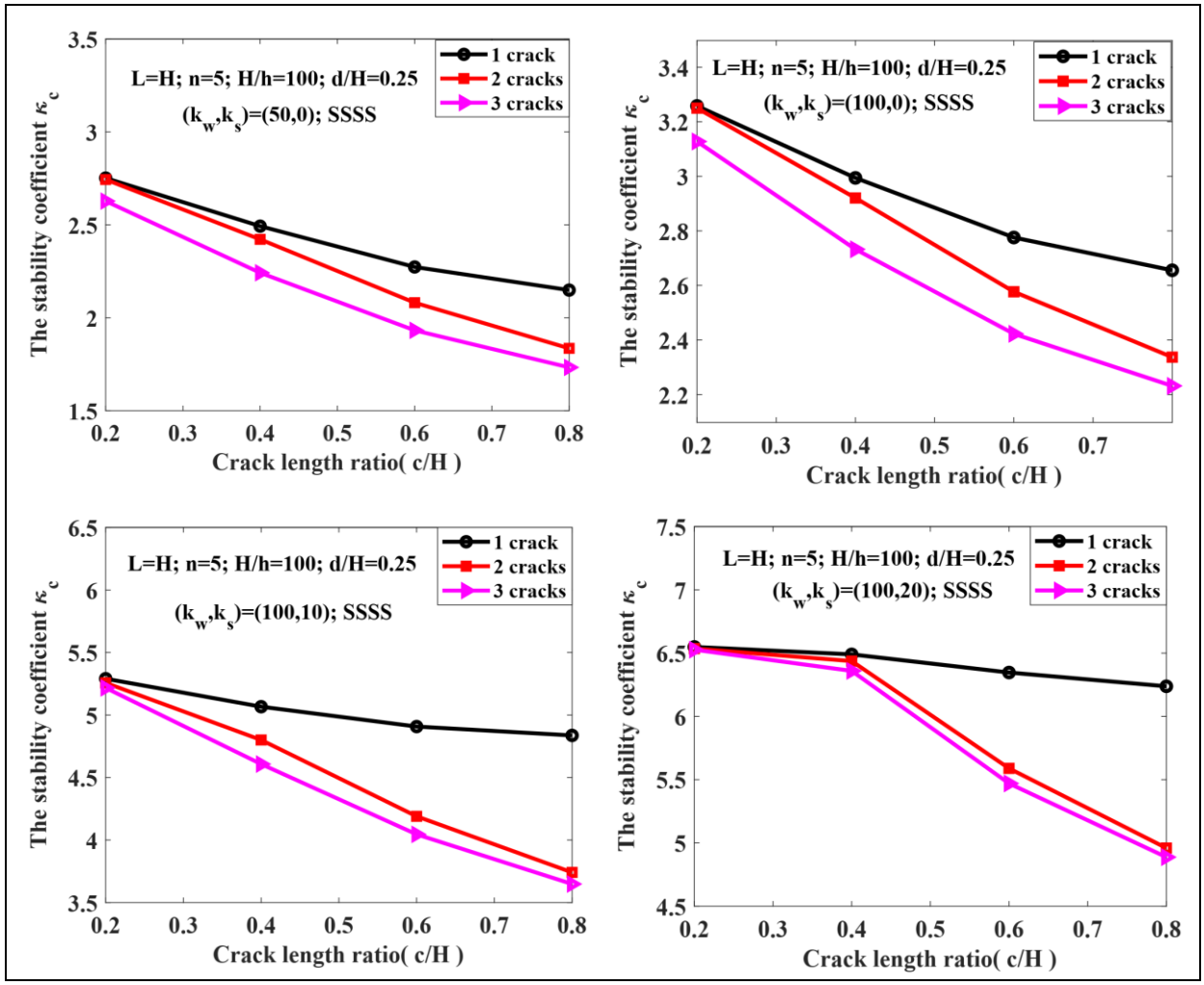

Figure 3. The cracked FG plate with many cracks on elastic foundation with $L=H$; ; H/h = 100; d/H=0.25; n = 5; *SSSS*.

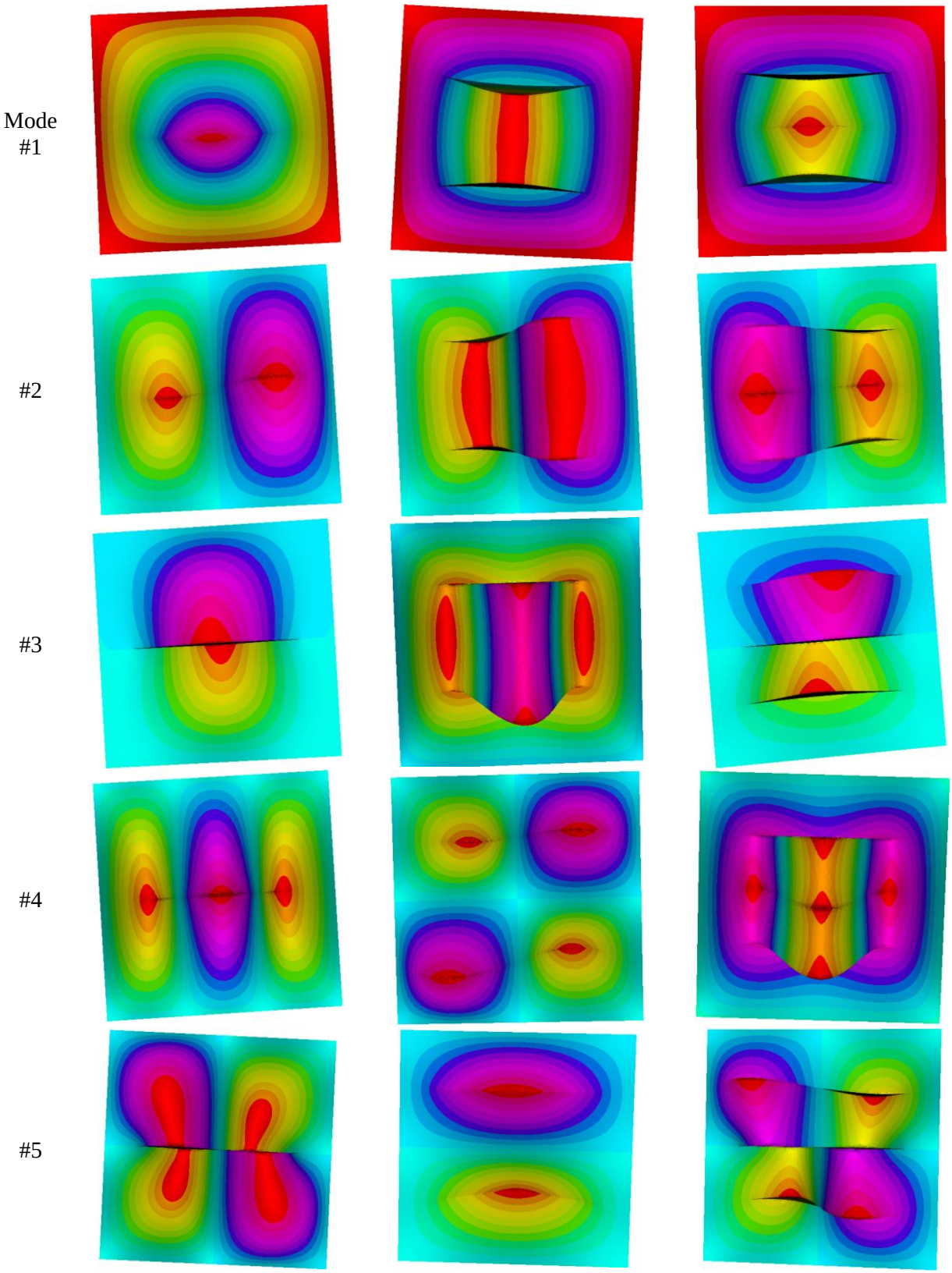

a. Plate with a crack b. Plate with 2 cracks c. Plate with 3 cracks

Figure 4. The first five types of instability cracked FG plate placed on elastic foundation $L=H$; $\tilde{k}_w = 50; \tilde{k}_s = 5$; ; H/h = 100; c/H=0.7; d/H=0.25; n = 3; *SSSS*.

In the next problem, the experiment is set up by keeping the volume index (n), the distance between the cracks (d) constant and changing both the number of cracks and the elastic matrix parameter as shown in Fig. 3, the impact from the number of cracks is evident in this section. It is clear that the plate with a crack has the greatest destabilization force. In particular, with the slab placed on the foundation with additional shear resistance coefficient k_s (Pasternak foundation), the number of cracks has a great influence.

Figure 4 presents the first five buckling types of cracked FG plates placed on an elastic foundation with cases of 1 crack, 2 cracks and 3 cracks parallel to the x-axis. It can be seen that the number of cracks has a significant influence on the shape of the buckling forms of the plate.

4. CONCLUSION

Using the theory of phase field theory and HSDT proposed by Shi [18], the paper has proposed a new approach to study the unstable behavior of FG plates with many traces internal cracks, especially plates placed on the Pasternak elastic foundations. In this paper, the plate is placed under compression on opposite sides along the x-axis, also known as uniaxial compression. The influences of the power-law index (n), the number of cracks with their location, the crack length, as well as the elastic background change on the critical buckling load were analyzed. When the power-law index (n) is increased or the crack length (c) is increased, the critical buckling load is reduced and the plate is prone to buckling; conversely, when the gap between cracks is widened, the critical load increases (provided that the plate is placed on the Winkler foundation). The study also shows that the elastic foundation has a very positive effect on the load-carrying capacity of the plate, when the Pasternak coefficient increases, the stiffness of the foundation increases, making the plate now have a higher stiffness, so the stability coefficient of the plate increases. The numerical solution of the buckling load obtained has high reliability and good agreement with the reference calculation results for thin plates with internal cracks. Last but not least, the present numerical study opens up new possibilities for further investigation of other problems such as the problem of nonlinear buckling in the plate when simultaneously applied loads such as thermal and mechanical load, or the problem of instability as the crack grows.

ACKNOWLEDGMENT

This research is funded by University of Transport and Communications (UTC) under grant number T2023-CB-002.

REFERENCES

[1]. Hiroyuki Matsunaga, Vibration and Stability of Thick Plates on Elastic Foundations, Journal of engineering mechanics, 126 (2000) 27-34. https://doi.org/10.1061/(ASCE)0733-9399(2000)126:1(27)
[2]. Takuya Morimoto, Yoshinobu Tanigawa, Elastic stability of inhomogeneous thin plates on an elastic foundation, Arch. Appl. Mech., 77 (2007) 653–674. https://doi.org/10.1007/s00419-007-0117-1
[3]. Mehdi Dehghan, Gholam Hosein Baradaran, Buckling and free vibration analysis of thick rectangular plates resting on elastic foundation using mixed finite element and differential quadrature method, Applied Mathematics and Computation, 218 (2011) 2772-2784. https://doi.org/10.1016/j.amc.2011.08.020
[4]. Huu-Tai Thai, Seung-Eock Kim, Closed-form solution for bucking analysis of thick functionally graded plates on elastic foundation, International Journal of Mechanical Sciences, 75 (2013) 34-44. http://dx.doi.org/10.1016/j.ijmecsci.2013.06.007
[5]. H. Foroughi, M. Azhari, Mechanical buckling and free vibration of thick functionally graded

plates resting on elastic foundation using the higher order B-spline finite strip method, Meccanica, 49 (2014) 981–993. https://doi.org/10.1007/s11012-013-9844-2
[6]. A. Gupta, M. Talha, Static and Stability Characteristics of Geometrically Imperfect FGM Plates Resting on Pasternak Elastic Foundation with Microstructural Defect, Arab. J. Sci. Eng., 43 (2018) 4931-4947. https://doi.org/10.1007/s13369-018-3240-0
[7]. S. J. Singh, S. P. Harsha, Exact solution for Free Vibration and Buckling of sandwich S-FGM Plates on Pasternak Elastic Foundation with Various Boundary Conditions, International Journal of Structural Stability and Dynamics, 19 (2019) 1-35. https://doi.org/10.1142/S0219455419500287
[8]. J. Jędrysiak, M. Kaźmierczak-Sobińska, Theoretical Analysis of Buckling for Functionally Graded Thin Plates with Microstructure Resting on an Elastic Foundation, Materials, 13 (2020) 1-20. https://doi.org/10.3390/ma13184031
[9]. Nicolas Moës, John Dolbow, Ted Belytschko, A finite element method for crack growth without remeshing, Int. J. Numer. Meth. Engng, 46 (1999) 131-150. https://doi.org/10.1002/(SICI)1097-0207(19990910)46:1<131::AID-NME726>3.0.CO;2-J
[10]. Amir Nasirmanesh, Soheil Mohammadi, XFEM buckling analysis of cracked composite plates, Composite Structures, 131 (2015) 333-343. https://doi.org/10.1016/j.compstruct.2015.05.013
[11]. C.S. Huang, O.G. McGee, M.J. Chang, Vibrations of cracked rectangular FGM thick plates, Composite Structures, 93 (2011) 1747-1764. https://doi.org/10.1016/j.compstruct.2011.01.005
[12]. P. Liu, T.Q. Bui, D. Zhu, T.T. Yu, J.W. Wang, S.H. Yin, S. Hirose, Buckling failure analysis of cracked functionally graded plates by a stabilized discrete shear gap extended 3-node triangular plate element, Composites Part B: Engineering, 77 (2015) 179-193. https://doi.org/10.1016/j.compositesb.2015.03.036
[13]. P.M. Phuc, N.D. Duc, The effect of cracks on the stability of the functionally graded plates with variable-thickness using HSDT and phase-field theory, Composites Part B: Engineering, 175 (2019) 107086. https://doi.org/10.1016/j.compositesb.2019.107086
[14]. P.M. Phuc, N.D. Duc, The effect of cracks and thermal environment on free vibration of FGM plates, Thin–Walled Structures, 159 (2021) 107291. https://doi.org/10.1016/j.tws.2020.107291
[15]. N.D. Duc, P.M. Phuc, Free vibration analysis of cracked FG CNTRC plates using phase field theory, Aerospace Science and Technology, 112 (2021) 106654. https://doi.org/10.1016/j.ast.2021.106654
[16]. Pham Minh Phuc, Analysis free vibration of the functionally grade material cracked plates with varying thickness using the phase-field theory, Transport and Communications Science Journal, 70 (2019) 122-131. https://doi.org/10.25073/tcsj.70.2.35
[17]. Pham Minh Phuc, Using phase field and third-order shear deformation theory to study the effect of cracks on free vibration of rectangular plates with varying thickness, Transport and Communications Science Journal, 71 (2020) 853-867. https://doi.org/10.47869/tcsj.71.7.10
[18]. G. Shi, A new simple third-order shear deformation theory of plates, International Journal of Solids and Structures, 44 (2007) 4399-4417. https://doi.org/10.1016/j.ijsolstr.2006.11.031
[19]. M.J. Borden, C.V. Verhoosel, M.A.Scott, T.J.R. Hughes, C.M. Landis, A phase-field description of dynamic brittle fracture, Comput Methods Appl Mech Eng, 217–220 (2012) 77–95. https://doi.org/10.1016/j.cma.2012.01.008